

Event-by-event distribution of the ratio of magnetic field energy to initial fluid energy density in $\sqrt{s_{NN}} = 200$ GeV Au-Au collisions

Victor Roy and Shi Pu

Institute for Theoretical Physics, Goethe University, Max-von-Laue-Str. 1, 60438 Frankfurt am Main, Germany

(Received 7 September 2015; revised manuscript received 2 November 2015; published 3 December 2015)

We estimate the event-by-event (e-by-e) distribution of the ratio (σ) of the magnetic and electric field energy density to the fluid energy density in the transverse plane of Au-Au collisions at $\sqrt{s_{NN}} = 200$ GeV. A Monte Carlo (MC) Glauber model is used to calculate σ in the transverse plane for impact parameter $b = 0, 12$ fm at time $\tau_i \sim 0.5$ fm. The fluid energy density is obtained by using Gaussian smoothing with two different smoothing parameter $\sigma_g = 0.25, 0.5$ fm. For $b = 0$ fm collisions σ is found to be $\ll 1$ in the central region of the fireball and $\sigma \gtrsim 1$ at the periphery. For $b = 12$ fm collisions $\sigma \gtrsim 1$ is observed for some events. The e-by-e correlation between σ and the fluid energy density (ε) is studied. We did not find strong correlation between σ and ε at the center of the fireball, whereas they are mostly anticorrelated at the periphery of the fireball.

DOI: [10.1103/PhysRevC.92.064902](https://doi.org/10.1103/PhysRevC.92.064902)

PACS number(s): 25.75.Ag

I. INTRODUCTION

The most strongest known magnetic field ($B \sim 10^{18}-10^{19}$ Gauss) in the universe is produced in laboratory experiments of Au-Au or Pb-Pb collisions in the collider experiments at the BNL Relativistic Heavy Ion Collider (RHIC) and at the CERN Large Hadron Collider (LHC). Previous theoretical studies show that the intensity of the produced magnetic field rises approximately linearly with the center of mass energy ($\sqrt{s_{NN}}$) of the colliding nucleons [1,2]. The Lorentz boosted electric fields in such collisions also become very strong which is the same order of magnitude as the magnetic field ($e\vec{B} \approx e\vec{E} \sim 10m_\pi^2$ for a typical Au-Au collision at top RHIC energy $\sqrt{s_{NN}} = 200$ GeV) [3], where m_π is the pion mass. Such intense electric and magnetic fields are strong enough to initiate the particle production from vacuum via Schwinger mechanism [4]. Using quantum chromodynamics it was shown in Ref. [5] that beyond a critical value of magnetic field the quark-antiquark state can possibly attain negative mass (in the limit of large number of colors). Thus it is important to know if there is truly an upper limit of magnetic field intensity allowed by the quantum chromodynamics when applied in heavy ion collisions, or the magnetic field can grow to arbitrary large value with increasing $\sqrt{s_{NN}}$ as predicted in some earlier studies [1,2]. In this work we shall calculate the electromagnetic field intensity without considering any such constraints, i.e., we assume that the electric and magnetic fields can attain any arbitrary large values.

There are several other interesting recent studies related to the effect of ultra-intense magnetic fields in heavy-ion collisions. Here we briefly mention a few of them which might be relevant to the present study. In the presence of a strong magnetic field as created in heavy-ion collisions, a charge current is induced in the quark gluon plasma (QGP), leading to what is known as the ‘‘chiral magnetic effect’’ (CME) [6]. Within a 3+1-dimensional anomalous hydrodynamics model a charge dependent hadron azimuthal correlations was found to be sensitive to the CME in Ref. [7]. Along with CME, it was also predicted theoretically that massless fermions with the same charge but different chirality will be separated,

yielding what is called the ‘‘chiral separation effect’’ (CSE). A connection between these effects and the Berry phase in condensed matter was also pointed out in Refs. [8–10]. In the hadronic phase a significant change in the hadron multiplicity was observed in the presence of a strong magnetic field within a statistical hadron resonance gas model in Ref. [11]. There are a lot of other important relevant works in this new emerging field which we cannot refer here, one can see recent reviews on this topic in Refs. [12–14] for more details.

The relativistic hydrodynamic models have so far nicely explained the experimentally measured anisotropic particle production in the azimuthal directions in heavy ion collisions. The success of the hydrodynamics model shows that a locally equilibrated QGP with small ratio of shear viscosity to entropy density is formed after the collision within a short time interval $\sim 0.2-0.6$ fm [15–21]. It is also well known that the final momentum anisotropy in hydrodynamic evolution is very sensitive to the initial (geometry) state of the nuclear collisions. So far almost all the hydrodynamic models studies have neglected any influence of magnetic fields on the initial fluid energy density or on the space-time evolution of QGP. But as we know the initial magnetic field is quite large, it is important to investigate the relative importance of a large electromagnetic field on the usual hydrodynamical evolution of QGP. For that one needs a full 3+1-dimensional magnetohydrodynamic code to numerically simulate the space-time evolution of QGP with magnetic fields. While one can gain some insight about the relative importance of the magnetic field on the initial energy density of the QGP fluid by estimating the quantity plasma σ , which is the dimensionless ratio of magnetic field energy $\frac{(eB)^2}{2}$ to the fluid energy density (ε): $\sigma = \frac{(eB)^2}{2\varepsilon}$. In plasma $\sigma \sim 1$ indicates that one can no longer neglect the effect of magnetic fields in the plasma evolution (in some situation $\sigma \sim 0.01$ may also affect the hydrodynamic evolution) [22–25]. In the present study we use Monte Carlo (MC) Glauber model [26,27] to calculate event-by-event (e-by-e) magnetic fields and fluid energy density for Au-Au collisions at $\sqrt{s_{NN}} = 200$ GeV and investigate the relative importance of the magnetic field on initial fluid energy density.

As mentioned earlier, the typical magnetic field produced in midcentral Au-Au collisions at $\sqrt{s_{NN}} = 200$ GeV reaches $\sim 10m_{\pi}^2$, which corresponds to field energy density of ~ 5 GeV/fm³. Hydrodynamical model studies show that the initial energy density for such cases is ~ 10 GeV/fm³, thus implying $\sigma \sim 0.2$ under these conditions. However, the magnetic field produced at the time of collisions decays very quickly if QGP does not possess finite electrical conductivity [28,29,32]. Thus in order to correctly estimate σ , one needs to consider the proper temporal evolution of magnetic fields until the thermalisation time ($\tau_i \sim 0.5$ fm for Au-Au collisions at RHIC) when the hydrodynamic evolution starts. Since the spatial distribution of fluid energy density as well as the electromagnetic fields varies e-by-e we also calculate σ accordingly. The spatial distribution of electric and magnetic fields in heavy ion collisions was previously studied in Refs. [30,31].

In the present work we study the spatial distribution of σ in $\sqrt{s_{NN}} = 200$ GeV Au-Au collisions for two different impact parameters ($b = 0$ and 12 fm). The temporal evolution of the magnetic fields after the collision is taken into account in a simplified manner which will be discussed in the next section. We also investigate the correlation between σ and fluid energy density in the transverse plane. The paper is organized as follows. In the next section, we discuss about the formalism. Our main result and discussion are presented in Sec. III. A summary is given at the end in Sec. IV.

II. FORMALISM AND SETUP

We constructed a spatial grid of size 10 fm in each direction (x and y) with the corresponding grid spacing of $\Delta x = \Delta y = 0.5$ fm for e-by-e calculation of electromagnetic fields and fluid energy density in the plane transverse to the trajectory of the colliding nuclei. The position of colliding nucleons are obtained from the MC-Glauber model in an e-by-e basis. The position of nucleons are randomly distributed according to the Woods-Saxon nuclear density distribution (as shown in Fig. 1). We adopt the usual convention used in heavy ion collisions for describing the geometry of the nuclear collisions, i.e., the impact parameter vector (\vec{b}) of the collision is along x axes and the colliding nuclei are symmetrically situated around the (0,0) point of the computational grid. The electric and magnetic fields at point $\vec{r}(x, y)$ at time t due to all charged protons inside two colliding nucleus are calculated from the Lienard-Weichart formula

$$\vec{E}(\vec{r}, t) = \frac{e}{4\pi} \sum_{i=1}^{N_{\text{proton}}} Z_i \frac{\vec{R}_i - R_i \vec{v}_i}{(R_i - \vec{R}_i \cdot \vec{v}_i)^3} (1 - v_i^2), \quad (1)$$

$$\vec{B}(\vec{r}, t) = \frac{e}{4\pi} \sum_{i=1}^{N_{\text{proton}}} Z_i \frac{\vec{v}_i \times \vec{R}_i}{(R_i - \vec{R}_i \cdot \vec{v}_i)^3} (1 - v_i^2), \quad (2)$$

where \vec{E} and \vec{B} are the electric and magnetic field vectors, respectively, e is the charge of a proton, Z is the number of proton inside each nucleus, $\vec{R}_i = \vec{x} - \vec{x}_i(t)$ is the distance from a charged proton at position \vec{x}_i to \vec{x} where the field is evaluated, \vec{v}_i is the velocity of the i th proton inside the colliding nucleus.

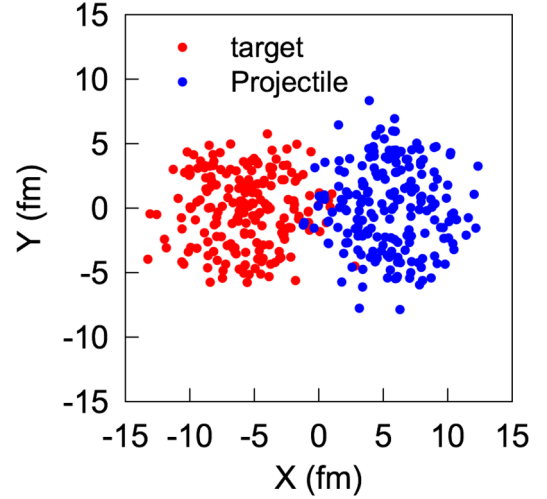


FIG. 1. (Color online) Distribution of nucleons inside target and projectile nuclei in typical Au-Au collisions at $\sqrt{s_{NN}} = 200$ GeV for $b = 12$ fm.

R_i is the magnitude of \vec{R}_i . The summation runs over all proton (N_{proton}) inside the two colliding nuclei. Following Ref. [1] we assume that because of the large Lorentz factor ($\gamma \sim 100$) the colliding nuclei are highly Lorentz contracted along the z direction and all the colliding protons have same velocity $v_i^{\text{first}} = (0, 0, v_z)$ and $v_i^{\text{second}} = (0, 0, -v_z)$. v_z is related to the c.m.

energy ($\sqrt{s_{NN}}$) through the relationship $v_z = \sqrt{1 - (\frac{2m_p}{\sqrt{s_{NN}}})^2}$, where m_p is the proton mass. Note that according to Eqs. (1) and (2) the electric and magnetic fields diverge as $\vec{R}_i \rightarrow 0$, to remove this singularity we assume a lower value $R_{\text{cut}} = 0.3$ fm as used in Ref. [1]. This particular value of $R_{\text{cut}} = 0.3$ fm was fixed as an effective distance between partons and it was found that the calculated electromagnetic field has weak dependence for $0.3 \text{ fm} \leq R_{\text{cut}} \leq 0.6 \text{ fm}$. We note that the quantities $e\vec{B}$ and $e\vec{E}$ has dimension GeV² and the conversion from GeV² to Gauss is given by $1 \text{ GeV}^2 = 5.12 \times 10^{19} \text{ Gauss}$.

It is customary to use Milne co-ordinate [$\tau = \sqrt{(t^2 - z^2)}$, $x, y, \eta = \frac{1}{2} \ln(\frac{t+z}{t-z})$] in heavy ion collisions. For our case we shall concentrate on the midrapidity region ($z \approx 0$) where $t \sim \tau$.

By using the MC-Glauber model we also compute the fluid energy density in the transverse plane from the position of wounded nucleons. This is a common practice to initialize energy density for e-by-e hydrodynamics simulations. Since the positions of the wounded nucleons (N_{wound}) are like a δ function in co-ordinate space, in order to calculate the energy density profile for hydrodynamics simulations one needs to smooth the initial profile by introducing Gaussian smearing for every colliding nucleon. The fluid energy density ε is parametrized as

$$\varepsilon(x, y, \sigma_g, \vec{b}) = k \sum_{i=1}^{N_{\text{wound}}} e^{-\frac{(x-x_i(\vec{b}))^2 + (y-y_i(\vec{b}))^2}{2\sigma_g^2}}. \quad (3)$$

Here, x, y is the co-ordinate of the computational grid, $x_i(\vec{b}), y_i(\vec{b})$ are the co-ordinates of wounded nucleons for an

impact parameter \vec{b} , σ_g is the Gaussian smearing which is taken to be 0.5 fm (unless stated otherwise) for our calculation. k is a constant which is tuned to match the initial central energy density for the event averaged case. We estimate $k = 6$ which results in the initial central energy density $40 \text{ GeV}/\text{fm}^3$ for $b = 0 \text{ fm}$ collision. This is the typical value of initial energy density used in the e-by-e hydrodynamics model to reproduce the experimental measured charged particle multiplicity in Au-Au collisions at $\sqrt{s_{NN}} = 200 \text{ GeV}$ for an initial time $\tau_i \sim 0.5 \text{ fm}$ [18]. The same k factor is used to calculate the initial energy density for all other impact parameters.

Once we calculate the electromagnetic field and the fluid energy density in the transverse plane, the plasma $\sigma(x, y, \vec{b}) = \frac{(eB(x, y, \vec{b}))^2}{2\varepsilon(x, y, \vec{b})}$ is readily obtained for each event. For our case we only considered the transverse components B_x and B_y to calculate the total magnetic energy density, since $B_z \ll B_x, B_y$. As mentioned, the hydrodynamics expansion of the QGP fluid starts after a time $\sim 0.5 \text{ fm}$, and because of the relativistic velocities of the charged protons the produced magnetic fields decays very quickly. If there is no conducting medium then the magnetic field decays as $\sim t^{-3}$. But in the presence of a conducting medium the decay can be substantially delayed [32]. However, the thermodynamic and transport properties of the nuclear matter right after the collision up to the time when the system reaches local thermal equilibrium are poorly known. Thus we investigate in our study two different scenarios when calculating $\sigma(x, y, \vec{b})$. From now on we will omit \vec{b} in the expression of σ , and because of spherical symmetry of the colliding nuclei we omit the vector arrow and simply write b for the impact parameter.

(i) In the first scenario, following Ref. [32] we assume that the matter in the pre-equilibrium phase has finite electrical conductivity and the field components are evaluated at $\tau_i = 0.5 \text{ fm}$ by reducing the magnitudes of the initial magnetic field (at $\tau = 0 \text{ fm}$) to 0.1 times. This is a simplification of the actual scenario, since the time evolution of the fields depend on the electrical conductivity, the impact parameter, and on the Lorentz gamma (γ) of the collisions. According to Ref. [32] the initial electromagnetic field produced in a $b = 7 \text{ fm}$ collision and for an electrical conductivity $\sigma_{el} = 5.8 \text{ MeV}$ reduced $\sim 50\%$ to its original value after $\tau \sim 0.5 \text{ fm}$. Note that for simplification in the numerical simulation we have ignored the impact parameter dependence of the evolution of the electromagnetic field in medium as was discussed in Ref. [32]. We note that according to lattice QCD and perturbative QCD studies QGP possesses finite temperature-dependent σ_{el} [33–35]. Similar temperature dependence of σ_{el} in the QGP phase was also found from a strongly coupled holographic calculation, for example, see Refs. [36–38], and references therein.

(ii) In the second scenario, we assume the magnetic field is evolved in vacuum (zero electrical conductivity) until the hydrodynamics expansion starts. For this case we reduced the magnitude of the initial electromagnetic field 0.01 times.

We note that in reality the situation may lie in between the above-mentioned two scenarios. From now on we denote the first and second scenarios by medium and vacuum, respectively.

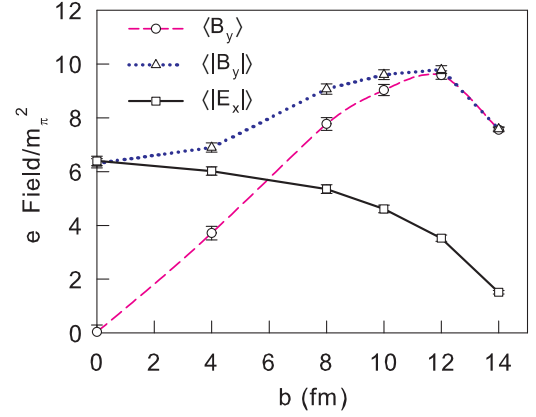


FIG. 2. (Color online) Impact parameter dependence of event averaged magnetic and electric fields at the center of the fireball for Au-Au collisions at $\sqrt{s_{NN}} = 200 \text{ GeV}$.

We consider 1000 nucleus-nucleus collisions for our present calculation for each impact parameter.

III. RESULTS AND DISCUSSION

At first we shall concentrate on the electromagnetic fields computed at the center of the fireball (i.e., at point $x = y = 0$ in our computational grid). Figure 2 shows the event averaged value of magnetic and electric fields as a function of impact parameter b . The B_y , its absolute value $|B_y|$, and x component of the electric field E_x are shown by pink dashed, blue dotted, and black solid lines, respectively. We note that our result is consistent with the result of Ref. [1]. We also checked other components of electric and magnetic fields and they are found to be consistent with Ref. [1].

The electric and magnetic fields are created in high energy heavy-ion collisions in presence of the electrically charged protons inside the two colliding nucleus. Whereas both neutron and protons inside the colliding nuclei deposit energy in the collision zone as a result of elastic and inelastic collisions among them. Since the positions of protons in the colliding nucleus is different with that of the positions of all nucleons, the resulting spatial distribution of the electromagnetic field is expected to differ from that of the initial fluid energy density. Figure 3 shows the event averaged value of fluid energy density at point ($x = y = 0$) as a function of impact parameter b . The energy density is obtained from Eq. (3) for $k = 6$. This specific value of k was chosen in order to obtain the central energy density $\sim 40 \text{ GeV}/\text{fm}^3$ for $b = 0 \text{ fm}$ collisions. From previous studies [18] we note that the initial central energy density for central (0–5% centrality which corresponds to $b \sim 2 \text{ fm}$) Au-Au collisions requires $\varepsilon \sim 40 \text{ GeV}/\text{fm}^3$ at initial time $\tau_i = 0.6 \text{ fm}$ at the center of the fireball ($x = y = 0$) to reproduce the experimentally measured charged hadron multiplicity at $\sqrt{s_{NN}} = 200 \text{ GeV}$. However, we note that a different initial time (τ_i) will give different initial energy density [39], in that case the magnitude of magnetic field at τ_i will also be different. From Figs. 2 and 3 we notice that fluid energy density decreases whereas the intensity of magnetic

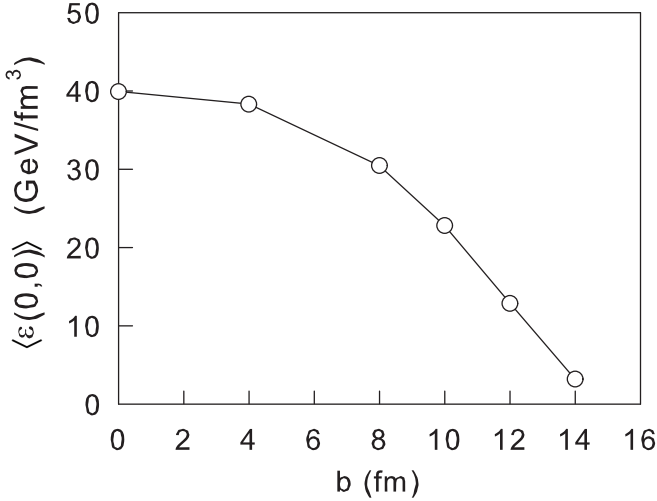


FIG. 3. Impact parameter dependence of event averaged central energy density ($\langle \varepsilon(0,0) \rangle$) of fluid for Au-Au collisions at $\sqrt{s_{NN}} = 200$ GeV.

field increases with b . It is thus expected that $\sigma(x,y,b)$ will reach its maximum value for $b \sim 12$ fm. So far we have shown the event average $\vec{E}(x,y)$, $\vec{B}(x,y)$, and $\varepsilon(x,y)$ at the center of the collision zone.

The top panel of Fig. 4 shows the event averaged $\varepsilon(x,y)$ for $b = 0$ fm collisions. Since the Au nucleus is almost spherical in shape, a head on Au-Au collision deposits energy in an almost circular zone. Different color schemes in the legend denote the energy density in units of GeV/fm³. The middle and bottom panels of Fig. 4 show the corresponding magnetic field energy density $\frac{(\vec{e}B)^2}{2}$ due to the y and x component of \vec{B} , respectively, where \vec{B} is calculated at time $\tau = 0$. We observe that the distribution of magnetic field energy is similar to the fluid energy density obtained from elastic and inelastic nucleon-nucleon collisions in the MC-Glauber model. The magnetic field energy density due to B_x and B_y is peaked at the center and has a SO(2) rotational symmetry for $b = 0$ fm collision. This is not surprising since the positions of the protons for $b = 0$ fm collisions have such rotational symmetry about the center of the fireball in the transverse plane for the event averaged case. The situation for a nonzero impact parameter collision becomes different. The overlap zone between the two nuclei becomes elliptical, as can be seen from the top panel of Fig. 5 which corresponds to $\varepsilon(x,y)$ for $b = 12$ fm. The middle and bottom panels of Fig. 5 show the corresponding energy density for B_y and B_x components. We find that the field energy density due to B_y has similar shape as fluid energy density, but that due to B_x has maximum in a dumbbell shaped region which is different from the initial fluid energy density.

So far we have shown the event averaged value of ε and components of \vec{B} . It is not clear from the above discussion whether the magnetic field energy density is negligible compared to the initial fluid energy density for every events because both ε and $\frac{(\vec{e}B)^2}{2}$ are lumpy in the transverse plane as shown in Fig. 6. This leads us to study $\sigma(x,y)$ on an e-by-e basis.

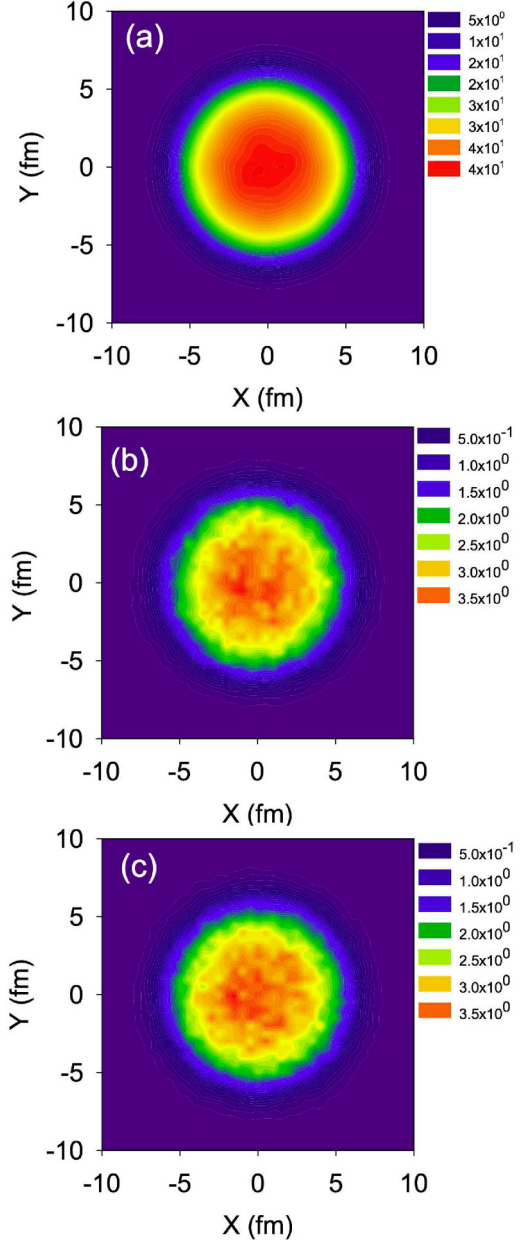


FIG. 4. (Color online) (a) 1000 event averaged initial energy density of QGP for $b = 0$ fm Au-Au collisions at $\sqrt{s_{NN}} = 200$ GeV. (b) 1000 event averaged magnetic field energy density calculated from the y component of the magnetic field for $b = 0$ fm Au-Au collisions at $\sqrt{s_{NN}}$ GeV. (c) Same as (b) but for the x component of the magnetic fields B_x .

A. Event-by-event $\sigma(x,y)$

The top panel of Fig. 6 shows the energy density, middle and bottom panels show corresponding $\sigma(x,y)$ at $\tau = 0.5$ fm for evolution of the magnetic field in medium and in vacuum, respectively, for a single event of $b = 12$ fm collisions. The shaded band in the middle and bottom panels correspond to the zones where $0.01 \leq \sigma(x,y) \leq 10$ (increasing in the outward direction). As expected $\sigma(x,y)$ reaches its maximum value in regions where $\varepsilon(x,y)$ becomes small.

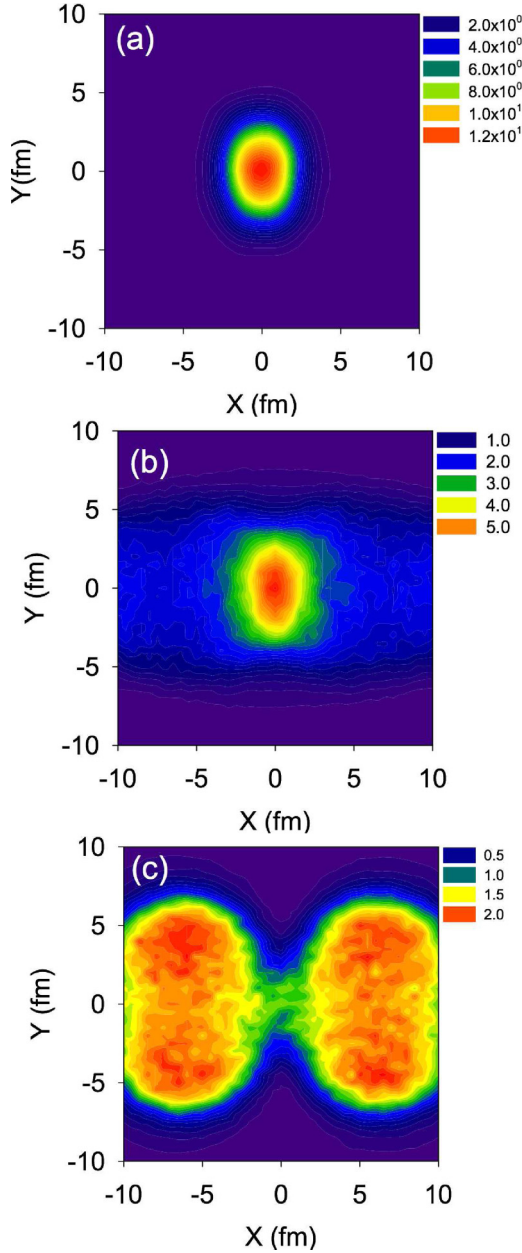


FIG. 5. (Color online) (a) 1000 event averaged initial energy density of QGP for Au-Au at $\sqrt{s_{NN}} = 200$ GeV for impact parameter $b = 12$ fm collisions. (b) event averaged magnetic field energy density calculated from the y component of the magnetic field for $b = 12$ fm Au-Au collisions at $\sqrt{s_{NN}}$ GeV. (c) Same as middle panel but for the x component of the magnetic fields B_x .

However, note that those regions of large $\sigma(x, y)$ strongly depend on the temporal evolution of the magnetic field from $\tau = 0$ fm until the hydrodynamics expansion starts at time τ_i . This can be seen from the bottom panel of the same figure where the regions of large $\sigma(x, y)$ moves outward as the magnetic field for this case decays faster than the case of medium with finite electrical conductivity.

We observe here that even if the magnetic field decays quickly (as in vacuum) until the hydrodynamics expansion starts, there is a corona of large $\sigma(x, y)$. It is then important to

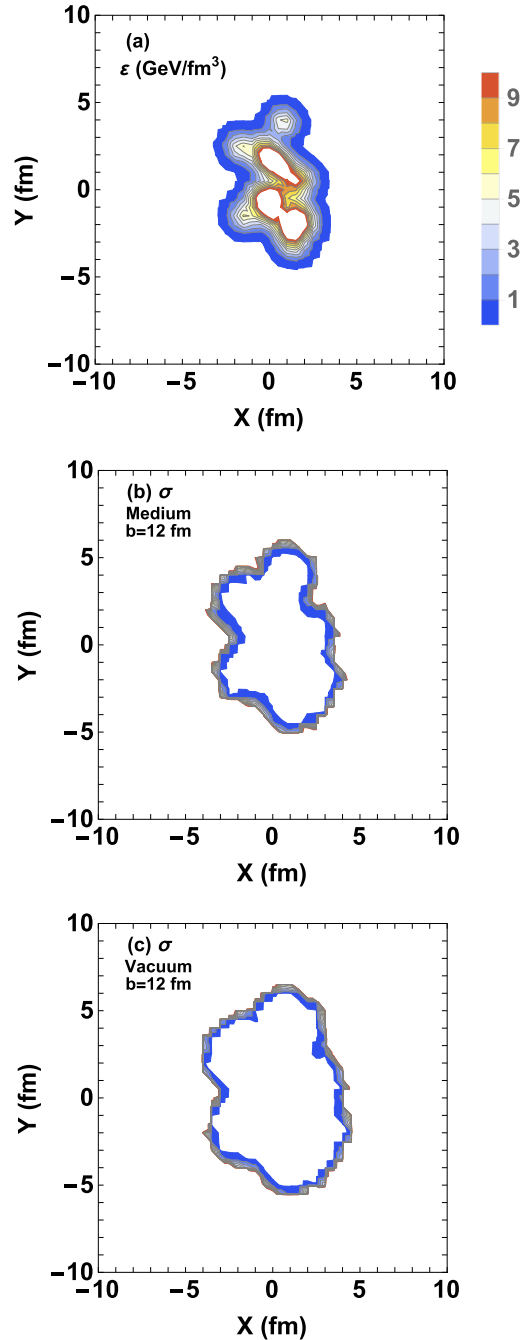


FIG. 6. (Color online) (a) Fluid energy density. (b) $\sigma(x, y)$ for the medium. (c) $\sigma(x, y)$ for the vacuum in a single $b = 12$ fm Au-Au $\sqrt{s_{NN}} = 200$ GeV collision. The shaded annular region in (b) and (c) corresponds to $0.01 \leq \sigma(x, y) \leq 10$.

consider the magnetohydrodynamics framework to investigate further the possible effects of those large $\sigma(x, y)$ zone on the space-time evolution of the QGP fluid. We expect that since the region of large σ seems to lie mostly outside the places where $\epsilon(x, y)$ is high there will be a minor modification in the transverse evolution of the QGP fluid when the effect of the magnetic field is taken into account. The above conclusion is made by investigating only one particular event, in order to

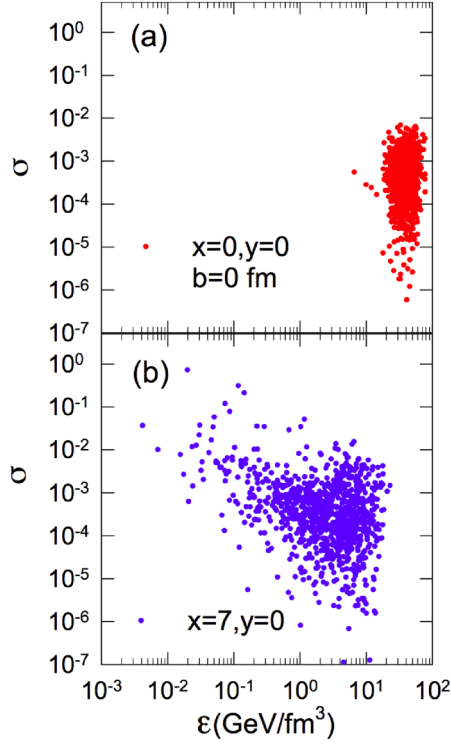


FIG. 7. (Color online) (a) e-by-e distribution of $\sigma(0,0)$ as a function of $\epsilon(0,0)$ for $b = 0$ fm Au-Au collisions at $\sqrt{s_{NN}} = 200$ GeV. (b) Same as (a) but for $(x = 7, y = 0)$.

understand the ensemble of events let us look at the e-by-e distribution of $\sigma(x,y)$ at the center ($x = y = 0$) and at the periphery of the collision zone.

Top panel of Fig. 7 shows the e-by-e distribution of $\sigma(0,0)$ as a function of $\epsilon(0,0)$ for $b = 0$ fm collisions. The bottom panel of the same figure shows the event distribution of $\sigma(7,0)$ versus $\epsilon(7,0)$. All results are obtained for magnetic field evolution in medium. Naively one expects that $\sigma(x,y)$ and $\epsilon(x,y)$ should be anticorrelated, i.e., for places where ϵ is large σ will be small and vice versa, the same conclusion was made in Ref. [31]. But it is clear from Fig. 7 that there is no such simple relationship between ϵ and σ for $b = 0$ fm collisions in the MC-Glauber model. In fact, we notice that at the center of the collision zone ϵ and σ are almost uncorrelated. For regions at the periphery of the collision zone (bottom panel) we observe similar behavior, but notice that here $\sigma(7,0)$ may reach ~ 1 in some events, whereas for $x = y = 0$ it never exceeds 0.01.

Now let us discuss the result for $b = 12$ fm collisions where the relative importance of the magnetic field is expected to be highest. The top panel of Fig. 8 shows the e-by-e distribution of $\sigma(0,0)$ as a function of $\epsilon(0,0)$ for $b = 12$ fm collisions. We notice that like $\sigma(0,0)$ distribution for $b = 0$ fm collisions, most of the events have $\sigma(0,0) \lesssim 0.01$. However, for few events $\sigma(0,0) \sim 1$. Like $b = 0$ fm collisions here we also notice no clear correlation between ϵ and σ . The bottom panel of Fig. 8 shows the distribution of $\sigma(3,0)$ as a function of $\epsilon(3,0)$. We notice that a considerable number of events have $\sigma \sim 1$ for this case.

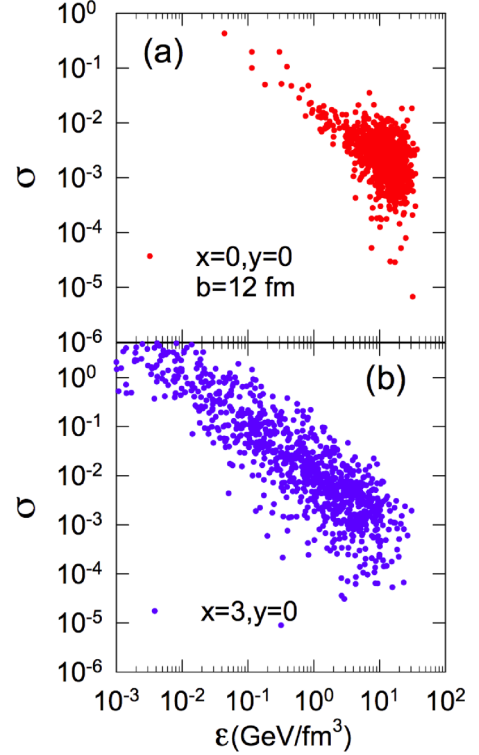


FIG. 8. (Color online) (a) e-by-e distribution of $\sigma(0,0)$ as a function of $\epsilon(0,0)$ for $b = 12$ fm Au-Au collisions at $\sqrt{s_{NN}} = 200$ GeV. (b) Same as top panel but for $(x = 3, y = 0)$.

Next we discuss the event averaged transverse profile of $\sigma(x,y)$ for $b = 0$ and 12 fm as depicted in Figs. 9 and 10, respectively. As expected, the event averaged $\sigma(x,y)$ in the range $0.01 \leq \sigma \leq 10$ for $b = 0$ fm collisions (Fig. 9) form an annular region enclosing the high energy density zone of the QGP fluid. The top panel of Fig. 9 shows the result for magnetic field evolution in vacuum and the bottom panel shows in medium. However, $\sigma(x,y)$ for $b = 12$ fm collisions shows different spatial distribution as depicted in Fig. 10. The nontrivial contour in this case results from the fact that for some events $\sigma(x,y)$ becomes very large and the event averaged value is dominated by those large σ . The top and bottom panels show the result for vacuum and medium, respectively.

B. Sensitivity of $\sigma(x,y)$ on Gaussian smearing

The Gaussian smearing σ_g in Eq. (3) is a free parameter which is usually taken in the range ~ 0.1 – 1.0 fm. Here we discuss the sensitivity of our result on Gaussian smearing by setting $\sigma_g = 0.25$ fm which is taken from a recent study [40]. Reducing σ_g results in very lumpy initial energy density hence we expect a different spatial dependence of $\sigma(x,y)$ compared to the previous case where $\sigma_g = 0.5$ fm is used. For $\sigma_g = 0.25$ fm we adjusted k to a new value $k = 17$ to keep the event-averaged initial central energy density for $b = 0$ fm collisions the same as before i.e., ~ 40 GeV/fm³. The top panel of Fig. 11 shows the e-by-e distribution of $\sigma(0,0)$ as a function of $\epsilon(0,0)$ for $b = 0$ fm Au-Au collisions. Bottom panel shows the same but for $x = 7, y = 0$. Comparing Figs. 7 and 11 we found

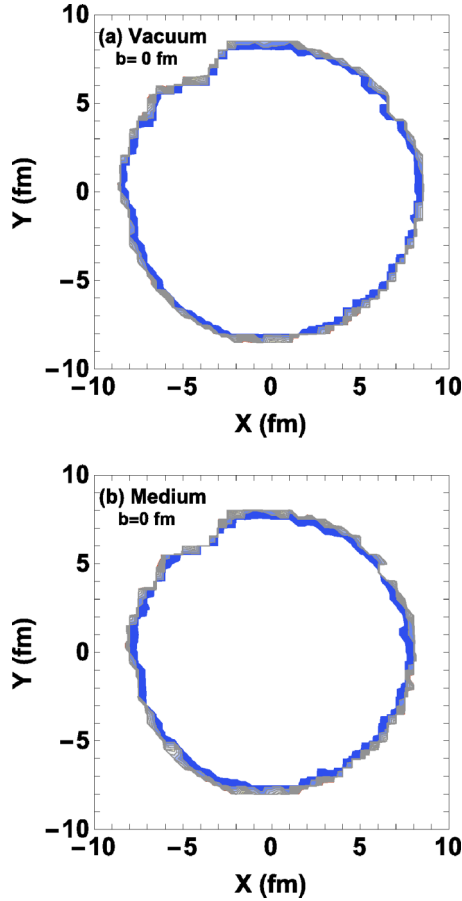


FIG. 9. (Color online) Event averaged $\sigma(x,y)$ in the range $0.01 \leq \sigma \leq 10$ (shaded region) for Au-Au collisions of $b = 0$ fm at $\sqrt{s_{NN}} = 200$ GeV. (a) For vacuum; (b) for medium.

that changing σ_g from 0.5 fm to 0.25 fm changes the e-by-e distribution of σ vs ε . Since the energy density is more lumpy for $\sigma_g = 0.25$ fm than 0.5 fm, the number of events with large σ increases. To see the effect of changed σ_g in peripheral collisions, we show the e-by-e distribution of σ vs ε for $b = 12$ fm in Fig. 12. The top panel of Fig. 12 shows the e-by-e distribution of $\sigma(0,0)$ vs $\varepsilon(0,0)$ and the bottom panel shows e-by-e distribution of $\sigma(3,0)$ vs $\varepsilon(3,0)$. It is clear that for $b = 12$ fm collisions the correlation between σ and ε at the center ($x = y = 0$) is sensitive to σ_g , and the maximum value of $\sigma \sim 1$, in contrary to what was observed for the case of $b = 0$ fm collisions.

C. Event-by-event $\sigma(x,y)$ due to electric fields

So far we have only discussed the ratio of magnetic field energy to the fluid energy density. Previously we have seen that the electric field in e-by-e Au-Au collisions is also comparable to the magnetic field. Thus it is worthwhile to investigate the ratio of electric field energy density to the fluid energy density $\sigma = \frac{(eE)^2}{2\varepsilon}$.

The top panel of Fig. 13 shows the e-by-e distribution of $\sigma(0,0)$ calculated for the electric field as a function of $\varepsilon(0,0)$ for $b = 0$ fm collisions. We notice that $\sigma(0,0)$ due to the

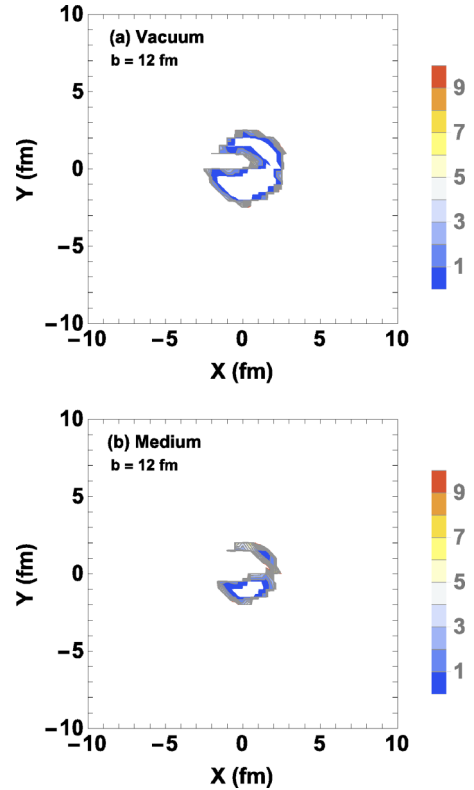


FIG. 10. (Color online) Event averaged $\sigma(x,y)$ in the range $0.01 \leq \sigma \leq 10$ (shaded region) for Au-Au collisions of $b = 12$ fm at $\sqrt{s_{NN}} = 200$ GeV. (a) For vacuum; (b) for medium.

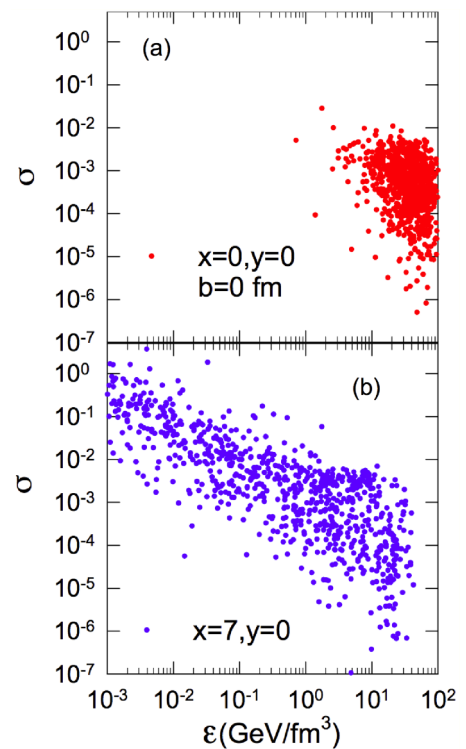


FIG. 11. (Color online) (a) e-by-e distribution of $\sigma(0,0)$ as a function of $\varepsilon(0,0)$ for Au-Au $b = 0$ fm collisions at $\sqrt{s_{NN}} = 200$ GeV. (b) Same as (a) but for $(x = 7, y = 0)$, $\sigma_g = 0.25$ for both cases.

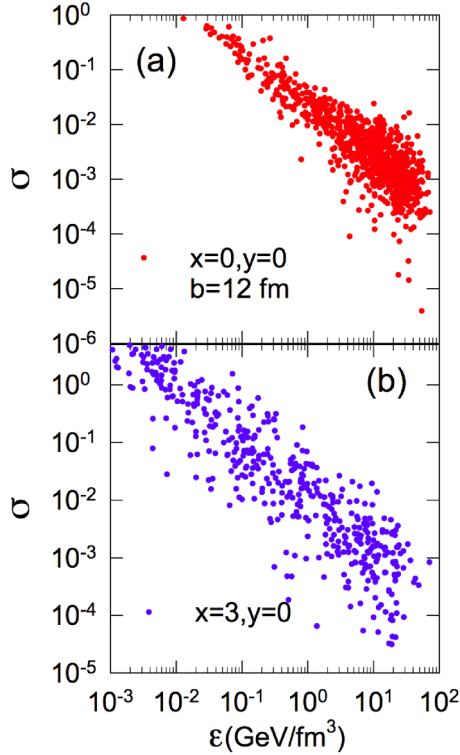


FIG. 12. (Color online) (a) e-by-e distribution of $\sigma(0,0)$ as a function of $\epsilon(0,0)$ for Au-Au $b = 12$ fm collisions at $\sqrt{s_{NN}} = 200$ GeV. (b) Same as (a) but for $(x = 3, y = 0)$. $\sigma_g = 0.25$ for both cases.

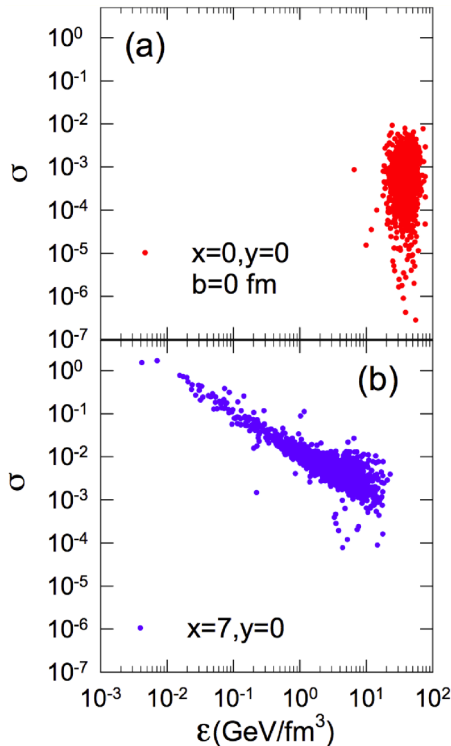


FIG. 13. (Color online) (a) e-by-e distribution of $\sigma(0,0)$ computed from the electric fields as a function of $\epsilon(0,0)$ for Au-Au $b = 12$ fm collisions at $\sqrt{s_{NN}} = 200$ GeV. (b) Same as (a) but for $(x = 7, y = 0)$. $\sigma_g = 0.5$ for both cases.

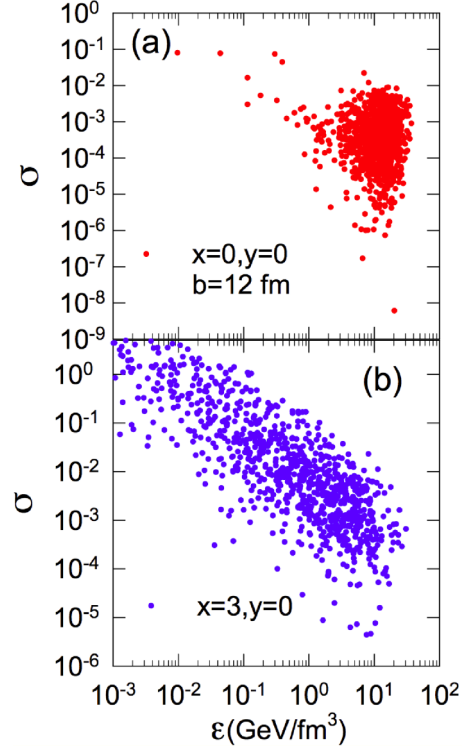


FIG. 14. (Color online) (a) e-by-e distribution of $\sigma(0,0)$ computed from electric fields as a function of $\epsilon(0,0)$ for Au-Au $b = 12$ fm collisions at $\sqrt{s_{NN}} = 200$ GeV. (b) Same as (a) but for $(x = 3, y = 0)$. $\sigma_g = 0.5$ for both cases.

electric field is small ($\lesssim 0.01$) and weakly correlated to the fluid energy density as was also observed for the magnetic fields. The bottom panel of Fig. 13 shows the same thing but for $x = 7, y = 0$. Compared to the case for the magnetic field (see Fig. 7), $\sigma(7,0)$ for an electric field shows strong correlation to the fluid energy density for $b = 0$ fm collisions. This is expected, since the electric field fluctuates less at the periphery as the electric fields from both the nuclei directed radially outward, whereas the magnetic fields from the two nuclei tend to cancel each other because they point in the opposite direction and hence fluctuates more compared to electric field. But for peripheral collisions the electric fields in the fireball from the colliding nuclei point in the opposite direction hence they show more fluctuation as can be seen for $b = 12$ fm collisions from the top and bottom panels of Fig. 14. Note that as for the case of magnetic fields, σ due to electric fields are also large for some events in the periphery of the fireball for peripheral collisions.

IV. SUMMARY AND DISCUSSION

We have studied the relative importance of magnetic and electric field energy on initial fluid energy density of the QGP by evaluating $\sigma = \frac{(eB)^2}{2\epsilon}$ and $\frac{(eE)^2}{2\epsilon}$ for Au-Au collisions at $\sqrt{s_{NN}} = 200$ GeV. The fluid energy density and electromagnetic fields are computed by using the MC-Glauber model using the following parameters: the cutoff distance $R_{cut} = 0.3$ fm, Gaussian smearing parameter $\sigma_g = 0.5$ (and 0.25 fm), and the scalar multiplicative factor $k = 6$ (and 17).

The initial energy density (at time $\tau_i = 0.5$ fm) for the fluid is fixed to ~ 40 GeV/fm³. The ratio of the magnetic and electric field energy density to the fluid energy density σ is evaluated in the transverse plane for two different impact parameters $b = 0$ and 12 fm. We find that for most of the events, at the center of the collision zone $\sigma(0,0) \ll 1$ for both $b = 0$ and 12 fm collisions. However, at the periphery of the collision zone where ε becomes small we observed a region of large σ . For large impact parameter collisions σ becomes larger for peripheral collisions (large b) compared to central (small b) collisions as a result of increase in magnetic field and decrease in fluid energy density. We observe that in central collisions ($b = 0$ fm) at the center of collision zone $\sigma \ll 1$ for most of the events. However, large σ is observed in the outer regions of the collision zone. In peripheral collisions σ becomes quite large at both the center and periphery of the collision zone. From this observation we conclude that initial strong magnetic fields might contribute to the total initial energy density of the Au-Au collisions (or other similar heavy ion collisions like Pb-Pb) significantly. However, the true effect of large σ (or large magnetic fields) will remain unclear unless one performs a realistic magnetohydrodynamics simulation with the proper initial conditions, for example see Refs. [22–25] for some theoretical estimates. We checked that the event averaged eccentricity of the initial energy density changes by $\sim 3.5\%$ for $b = 12$ fm collisions when one includes the magnetic fields. This change in initial state might effect the final elliptic and higher order flow in hydrodynamics simulations, and hence it may introduce further uncertainty in the extracted η/s obtained from the comparison of simulation and the experimental data for peripheral collisions as was also speculated in some previous studies [41,42]. A number of possible experimental observables, e.g. charge dependent azimuthal correlation, soft photon production among others, might be affected due to the azimuthally fluctuating electric and magnetic fields in heavy-ion collisions, for details see

Refs. [3,43,44] and references therein. Since the matter energy distribution changes when we include electromagnetic field energy in the matter distribution, it is worthwhile to check in a future study the possible effect of this change on the correlation of \vec{B} and the participant plane angle as done in a previous study [3]. On the other hand such a large σ also implies that those chiral phenomena, e.g., chiral magnetic effect, chiral separation effect, might not be ignorable in the hydrodynamic simulations. More systematical studies and simulations are required.

It is also worthwhile to mention that according to a recent study [45] the shear viscosity over entropy density ratio along the external magnetic field may violate the lower bound ($\frac{1}{4\pi}$) predicted by string theoretical and quantum mechanical calculations [46] which was also confronted by viscous hydrodynamics studies without an external magnetic field. Note that the results in this paper are obtained for a specific model of initial conditions (MC-Glauber model) with few free parameters. We have not explored all possible allowed values of these free parameters. In the future we can incorporate other initial conditions and a more realistic time evolution of the electromagnetic fields in the pre-equilibrium phase (as described in Ref. [32]) to study the effect of magnetic fields on initial fluid energy density distribution. It is also interesting to study the similar thing for lower $\sqrt{s_{NN}}$ collisions where the decay of a magnetic field in vacuum is supposed to be much slower than the present case because of the slower speed of the colliding nuclei, and also the corresponding initial energy density for such cases is smaller than the present case of Au-Au collisions at $\sqrt{s_{NN}} = 200$ GeV.

ACKNOWLEDGMENTS

V.R. and S.P. are supported by the Alexander von Humboldt Foundation, Germany. The authors would like to thank Dirk Rischke for discussion.

-
- [1] A. Bzdak and V. Skokov, *Phys. Lett. B* **710**, 171 (2012).
 - [2] W. T. Deng and X. G. Huang, *Phys. Rev. C* **85**, 044907 (2012).
 - [3] J. Błoczyński, X. G. Huang, X. Zhang, and J. Liao, *Phys. Lett. B* **718**, 1529 (2013).
 - [4] KEK Proceedings of the International Conference on Physics in Intense Fields (PIF 2010), November 24–26, 2010 Tsukuba, Japan, edited by K. Itakura, S. Iso, and T. Takahashi, <http://ccdb5fs.kek.jp/tiff/2010/1025/1025013.pdf>.
 - [5] Y. A. Simonov, B. O. Kerbikov, and M. A. Andreichikov, [arXiv:1210.0227](https://arxiv.org/abs/1210.0227) [hep-ph].
 - [6] D. E. Kharzeev, L. D. McLerran, and H. J. Warringa, *Nucl. Phys. A* **803**, 227 (2008).
 - [7] Y. Hirono, and E. Shuryak, *Phys. Rev. C* **91**, 054915 (2015).
 - [8] J. W. Chen, S. Pu, Q. Wang, and X. N. Wang, *Phys. Rev. Lett.* **110**, 262301 (2013).
 - [9] M. A. Stephanov and Y. Yin, *Phys. Rev. Lett.* **109**, 162001 (2012).
 - [10] D. T. Son and N. Yamamoto, *Phys. Rev. D* **87**, 085016 (2013).
 - [11] A. Bhattacharyya, S. K. Ghosh, R. Ray, and S. Samanta, [arXiv:1504.04533](https://arxiv.org/abs/1504.04533) [hep-ph].
 - [12] D. E. Kharzeev, *Prog. Part. Nucl. Phys.* **75**, 133 (2014).
 - [13] A. Bzdak, V. Koch, and J. Liao, *Lect. Notes Phys.* **871**, 503 (2013).
 - [14] D. E. Kharzeev, *Ann. Rev. Nucl. Part. Sci.* **65**, 193 (2015).
 - [15] C. Shen, S. A. Bass, T. Hirano, P. Huovinen, Z. Qiu, H. Song, and U. Heinz, *J. Phys. G* **38**, 124045 (2011).
 - [16] P. Romatschke and U. Romatschke, *Phys. Rev. Lett.* **99**, 172301 (2007); M. Luzum and P. Romatschke, *Phys. Rev. C* **78**, 034915 (2008).
 - [17] H. Song and U. W. Heinz, *Phys. Lett. B* **658**, 279 (2008); *Phys. Rev. C* **78**, 024902 (2008).
 - [18] V. Roy, A. K. Chaudhuri, and B. Mohanty, *Phys. Rev. C* **86**, 014902 (2012).
 - [19] H. Niemi, G. S. Denicol, P. Huovinen, E. Molnar, and D. H. Rischke, *Phys. Rev. C* **86**, 014909 (2012).
 - [20] U. Heinz, C. Shen, and H. Song, *AIP Conf. Proc.* **1441**, 766 (2012).
 - [21] B. Schenke, S. Jeon, and C. Gale, *Phys. Rev. C* **85**, 024901 (2012).
 - [22] M. Lyutikov and S. Hadden, *Phys. Rev. E* **85**, 026401 (2012).
 - [23] C. F. Kennel and F. V. Hadden, *Astrophys. J.* **283**, 694 (1984).

- [24] V. Roy, S. Pu, L. Rezzolla, and D. Rischke, *Phys. Lett. B* **750**, 45 (2015).
- [25] S. Pu, V. Roy, L. Rezzolla, and D. Rischke (unpublished).
- [26] Z. W. Lin, C. M. Ko, B. A. Li, B. Zhang, and S. Pal, *Phys. Rev. C* **72**, 064901 (2005).
- [27] M. L. Miller, K. Reygers, S. J. Sanders, and P. Steinberg, *Annu. Rev. Nucl. Part. Sci.* **57**, 205 (2007).
- [28] U. Gursoy, D. Kharzeev, and K. Rajagopal, *Phys. Rev. C* **89**, 054905 (2014).
- [29] B. G. Zakharov, *Phys. Lett. B* **737**, 262 (2014).
- [30] Y. Zhong, C. B. Yang, X. Cai, and S. Q. Feng, [arXiv:1507.07743](https://arxiv.org/abs/1507.07743) [hep-ph].
- [31] V. Voronyuk, V. D. Toneev, W. Cassing, E. L. Bratkovskaya, V. P. Konchakovski, and S. A. Voloshin, *Phys. Rev. C* **83**, 054911 (2011).
- [32] K. Tuchin, *Phys. Rev. C* **88**, 024911 (2013).
- [33] A. Amato, G. Aarts, C. Allton, P. Giudice, S. Hands, and J. I. Skullerud, *Phys. Rev. Lett.* **111**, 172001 (2013).
- [34] S. Gupta, *Phys. Lett. B* **597**, 57 (2004).
- [35] M. Greif, I. Bouras, C. Greiner, and Z. Xu, *Phys. Rev. D* **90**, 094014 (2014).
- [36] S. I. Finazzo and J. Noronha, *Phys. Rev. D* **89**, 106008 (2014).
- [37] S. Pu, S. Y. Wu, and D. L. Yang, *Phys. Rev. D* **89**, 085024 (2014).
- [38] S. Pu, S. Y. Wu, and D. L. Yang, *Phys. Rev. D* **91**, 025011 (2015).
- [39] C. Shen, U. Heinz, P. Huovinen, and H. Song, *Phys. Rev. C* **82**, 054904 (2010).
- [40] A. K. Chaudhuri, [arXiv:1507.04898](https://arxiv.org/abs/1507.04898) [nucl-th].
- [41] K. Tuchin, *J. Phys. G* **39**, 025010 (2012).
- [42] R. K. Mohapatra, P. S. Saumia, and A. M. Srivastava, *Mod. Phys. Lett. A* **26**, 2477 (2011).
- [43] J. Błoczynski, X. G. Huang, X. Zhang, and J. Liao, *Nucl. Phys. A* **939**, 85 (2015).
- [44] W. T. Deng and X. G. Huang, *Phys. Lett. B* **742**, 296 (2015).
- [45] R. Critelli, S. I. Finazzo, M. Zaniboni, and J. Noronha, *Phys. Rev. D* **90**, 066006 (2014).
- [46] G. Policastro, D. T. Son, and A. O. Starinets, *Phys. Rev. Lett.* **87**, 081601 (2001).